Dayside thermal inversion in the atmosphere of WASP-19b

A. S. Rajpurohit, F. Allard, D. Homeier, O. Mousis, S. Rajpurohit

A&A 642, A39 (2020)
https://doi.org/10.1051/0004-6361/202038302

Astronomy & Astrophysics

Dayside thermal inversion in the atmosphere of WASP-19b

A. S. Rajpurohit[1], F. Allard[2], D. Homeier[3], O. Mousis[4], and S. Rajpurohit[5]

[1] Astronomy & Astrophysics Division, Physical Research Laboratory, Navrangapura, Ahmedabad 380009, India
e-mail: arvindr@prl.res.in
[2] Univ. Lyon, ENS de Lyon, Univ. Lyon1, CNRS, Centre de Recherche Astrophysique de Lyon UMR 5574, 69007 Lyon, France
[3] Förderkreis Planetarium Göttingen e.V., Nordhäuser Weg 18, 37085 Göttingen, Germany
[4] Aix-Marseille Université, CNRS, LAM (Laboratoire d'Astrophysique de Marseille) UMR 7326, 13388 Marseille, France
[5] The Molecular Foundry, Lawrence Berkeley National Laboratory, Berkeley, CA 94720, USA

Received 30 April 2020 / Accepted 31 July 2020

ABSTRACT

Context. Observations of ultra-hot Jupiters indicate the existence of thermal inversion in their atmospheres, with dayside temperatures greater than 2200 K. Various physical mechanisms such as non-local thermal equilibrium, cloud formation, disequilibrium chemistry, ionisation, hydrodynamic waves, and associated energy have been omitted in previous spectral retrievals, while they play an important role in the thermal structure of their upper atmospheres.
Aims. We aim to explore the atmospheric properties of WASP-19b to understand its largely featureless thermal spectra using a state-of-the-art atmosphere code that includes a detailed treatment of the most important physical and chemical processes at play in such atmospheres.
Methods. We used the one-dimensional line-by-line radiative transfer code PHOENIX in its spherical symmetry configuration including the BT-Settl cloud model and C/O disequilibrium chemistry to analyse the observed thermal spectrum of WASP-19b.
Results. We find evidence for a thermal inversion in the dayside atmosphere of the highly irradiated ultra-hot Jupiter WASP-19b, with $T_{\rm eq} \sim 2700$ K. At these high temperatures we find that H_2O dissociates thermally at pressures below 10^{-2} bar. The inverted temperature-pressure profiles of WASP-19b show evidence of CO emission features at 4.5 μm in its secondary eclipse spectra.
Conclusions. We find that the atmosphere of WASP-19b is thermally inverted. We infer that the thermal inversion is due to the strong impinging radiation. We show that H_2O is partially dissociated in the upper atmosphere above about $\tau = 10^{-2}$, but is still a significant contributor to the infrared opacity, dominated by CO. The high-temperature and low-density conditions cause H_2O to have a flatter opacity profile than in non-irradiated brown dwarfs. Altogether these factors make H_2O more difficult to identify in WASP-19b. We suggest that the state-of-the-art PHOENIX model atmosphere code is well suited to the study of this new class of extrasolar planets, ultra-hot Jupiters.

Key words. radiative transfer – planets and satellites: gaseous planets – planets and satellites: atmospheres

1. Introduction

More than 4000 exoplanets have been discovered so far via detection techniques such as the transit and radial velocity methods. A large number of them fall into the category of hot Jupiters and are normally found around A, F, and G type stars (Zellem et al. 2017). In recent times, a new class of ultra-hot Jupiters has also been identified. Due to their close proximity to their host star, these ultra-hot Jupiters show distinct characteristics compared with hot Jupiters, such as a higher rate of transit and eclipse. Ultra-hot Jupiters with an orbital separation of less than 0.05 AU face the highest level of irradiation from their host stars. With large atmospheric scale heights, they display dayside temperatures ≥2200 K. Their short orbital periods and high temperature result in a high planet-to-star contrast ratio, particularly in the mid-infrared. This makes them ideal candidates to have their atmospheres probed (Burrows et al. 2004).

The atmospheres of hot Jupiters are predominantly composed of molecular hydrogen and atomic helium. Other significant molecules possibly found in their atmospheres are CO_2, C_2H_2, and HCN (Madhusudhan 2012). A recent study by Lothringer et al. (2018) showed that various atomic and molecular species such as O, C, N, Fe, Mg, H_2O, CO, CH_4, N_2, and NH_3, including SiO and metal hydrides, are also present at high temperatures in the atmospheres of hot Jupiters.

The wavelength dependence of the transit radii observations provides a measure of a planet's atmospheric composition (Fortney et al. 2003). For example, atomic sodium is detected from the transit radii observations of hot-Jupiter HD 209458b (Charbonneau et al. 2002) whereas H_2O has been detected in the atmosphere of both HD 189733b (Tinetti et al. 2007) and HD 209458b (Barman 2007). Observations of ultra-hot Jupiters have also revealed information about the thermal structure of their atmospheres (Madhusudhan et al. 2014).

Depending on the presence of an inverted or non-inverted thermal structure profile of their atmospheres, ultra-hot Jupiters can display emission or absorption features in their spectra. They may also show a blackbody spectrum in the presence of an isothermal profile (Fortney et al. 2008; Line & Parmentier 2016). The nature of the absorbers responsible for the thermal inversion in their atmospheres is not yet known, though the presence of vanadium oxide (VO) and titanium oxide (TiO) has been proposed as a cause for this (Burrows et al. 2008; Fortney et al. 2008). The observed absorption broadband features in their optical transmission spectrum between 0.62 and 0.8 μm can possibly be explained by these absorbers (Désert et al. 2008). Processes

such as vertical mixing that prevent the temperature inversion from occurring in their atmosphere are described by Spiegel et al. (2009) and Parmentier et al. (2013, 2016), whereas the role of stellar activity for the thermal inversion in the atmosphere of hot-Jupiters is studied by Knutson et al. (2010).

Evidence for the thermal inversion and diverse characteristics of the atmospheres of ultra-hot Jupiters are also imprinted in their near-infrared (NIR) observations. For example, TiO has been detected as an emission feature in WASP-33b (Haynes et al. 2015; Nugroho et al. 2017) and as an absorption feature in WASP-19b (Sedaghati et al. 2017). Emission features due to H_2O and VO have also been detected in WASP-121b (Evans et al. 2017). The presence of thermal inversion without H_2O, TiO, and VO has been noticed in the low resolution secondary eclipse spectra of WASP-18b (Sheppard et al. 2017; Arcangeli et al. 2018). Their study provides evidence for CO emission at 4.5 μm, implying an inverted thermal structure. On the other hand, no clear evidence for emission or absorption features of H_2O is found in HAT-P-7b (Mansfield et al. 2018), WASP-12b (Swain et al. 2013), and WASP-103b (Kreidberg et al. 2018). These planets instead show a thermal blackbody spectra. A handful of extremely hot Jupiters also do not show any hint of thermal inversion, such as HD 209458b, KELT-1b, and Kepler-13Ab (Diamond-Lowe et al. 2014; Beatty et al. 2017a,b).

Retrieval techniques are commonly used to constrain the chemical composition and thermal structure, and to explain the featureless spectra of ultra-hot Jupiters (Madhusudhan & Seager 2009; Line et al. 2013; Stevenson et al. 2014). Such methods enabled the detection of CO with a high C/O ratio in WASP-18b (Sheppard et al. 2017) and the derivation of a sub-solar metallicity associated with an oxygen-rich composition in WASP-33b (Haynes et al. 2015). A forward modelling approach (Arcangeli et al. 2018; Lothringer et al. 2018; Parmentier et al. 2018) explains the lack of strong H_2O spectral features in the ultra-hot Jupiters due to molecular dissociation. Considering H– opacity and the thermal dissociation of H_2O, Arcangeli et al. (2018), Kreidberg et al. (2018), Kitzmann et al. (2018), and Mansfield et al. (2018) explained the featureless spectra in some ultra-hot Jupiters for example HAT-P-7b, KELT-9b, WASP-12b, WASP-121b, and WASP-18b. Although the retrieval techniques are useful to quantify the atmospheric abundances of ultra-hot Jupiters, the results demonstrate a large diversity in their chemical composition and thermal structures, which could lead to biased conclusions.

In this paper, we investigate the atmospheric properties of the ultra-hot Jupiter WASP-19b. WASP-19b is among the objects that exhibit weaker spectral features compared to their cooler counterparts. WASP-19b has a shorter orbital period and, thus, receives extreme irradiation from its host star. Its atmosphere is then of particular interest to study. We argue that proper chemistry and opacity play a key role in understanding its extreme hot atmosphere without invoking unusual abundances.

2. Model construction

To model the atmosphere of WASP-19b, we used the BT-Settl model atmosphere described in Allard et al. (2012) and Rajpurohit et al. (2012). BT-Settl is a state-of-the-art model atmosphere code, which has been extremely successful in reproducing the properties of stellar to sub-stellar objects including cool brown dwarfs. The current version of the BT-Settl model uses H_2O along with other molecular line lists such as FeH, CrH, TiO, VO, CaH, NH_3, Mg, CO_2, and CO. Collision induced absorption (CIA) from H_2 collisions with H_2, He, CH_4, N_2, and Ar along with CO_2-CO_2, Ar-CH_4, and CH_4-CH_4 are also included (see Allard et al. 2012 for more detail). The BT-Settl model accounts for many continuous opacity sources, including bound-free opacity from H, H^-, He, C, N, O, Na, Mg, Al, Si, S, Ca, and Fe, free-free opacity from H, Mg, and Si, and scattering from e^-, H, He, and H_2. The model includes the opacities of more than 100 molecular species, including many molecules, isotopes, atomic species, and their ionised states. Detailed profiles for the alkali lines as described in Unsold (1968), Valenti & Piskunov (1996), and Allard et al. (2007) and approximation is utilised for the atomic damping constants with a correction factor to the widths of 2.5 for the non-hydrogenic atoms. Several important atomic transitions, such as the alkali, Ca I, and Ca II resonance lines along with more accurate broadening data for neutral hydrogen collisions by Barklem et al. (2000) have been included.

The BT-Settl model also accounts for disequilibrium chemistry for C/O and N (Graven & Long 1954; Visscher et al. 2010; Allard et al. 2012). The reference solar elemental abundances are derived from Caffau et al. (2011). These models are computed with version 15.5 of `PHOENIX`, a multi-purpose atmosphere code (Allard et al. 2001). `PHOENIX` solves the radiative transfer in 1D spherical symmetry with irradiation such that flux is conserved at each layer. The basic assumption in `PHOENIX` while solving radiative transfer is hydrostatic equilibrium with convection using the mixing length theory, and a sampling treatment of the opacities (see Allard et al. 2013).

The atmosphere model for WASP-19b irradiated by the host star of spectral type G5 with an orbital separation of 0.0163 AU has been computed by considering boundary conditions as described in Barman et al. (2001). A pre-computed converged non-irradiated model structure at 400 K is chosen from Allard et al. (2012) as the initial model structure to start with. The temperature is decreased down to 100 K to achieve the model structure. A temperature change of less than 1 K at every depth point in the thermal structure is considered as the criterion for the converged model. An effective temperature ($T_{\rm eff}$) of 5500 K, surface gravity ($\log g$) of 4.5, and [M/H]) = 0 have been taken as input parameters for the host star.

To explore and investigate the atmospheric properties of WASP-19b, models with uniform heat redistribution with $f = 0.5$ across the entire dayside have been calculated, with slanted rays for metallicity at –2.0, 0.0, and +2.0 dex. Here the factor f measures the uniform heat redistribution. Factor $f = 0.5$ indicates heat redistribution across the entire dayside while $f = 1$ indicates full heat redistribution. The model is calculated on an optical depth grid of 250 layers in log-space for $\tau = 10^{-9}$ to 10^3 at the peak of the spectral energy distribution that corresponds to pressures of 10^{-12} to ~10 bars. In the computation of the atmospheric model, some non-local thermal equilibrium (NLTE) processes have also been included for a small set of elements and level numbers (H I, He I, Li I, C I, Ni I, O I, Ne I, Na I, Na II, Mg I, Mg II, Si I, S I, K I, K II, Ca I, Ca II, Rb I), which affect the entire atmosphere. `PHOENIX` has been used to calculate both the planetary and stellar spectra from 10 to 10^6 Å. The planetary, stellar, and orbital parameters used for the computation irradiated model of WASP-19b are summarised in Table 1.

3. Results and discussion

A thermal spectrum of WASP-19b from Anderson et al. (2010), Anderson et al. (2013), Gibson et al. (2010), Burton et al. (2012), Bean et al. (2013), and Lendl et al. (2013), is shown in Fig 1. The planet-to-star flux ratio at 4.5 μm is higher than the one at the 3.6 μm *Spitzer*/IRAC channel. Moreover, at higher wavelengths,

Table 1. Planetary, stellar, and orbital parameters used in the model are from Butler et al. (2006), Southworth et al. (2007), Hebb et al. (2010), and Hellier et al. (2011).

Parameter	Value
a	0.0163 AU
$R_{[p]}$	1.386 ($R_{Jupiter}$)
$\log g_{[p]}$	3.17 [cm s^{-2}]
$T_{int[p]}$	100 [K]
$T_{eff[\star]}$	5500 [K]
$\log g_{[\star]}$	4.5 [cm s^{-2}]
$R_{[\star]}$	0.990 ($R_{\odot}$)
$[M/H]_{[\star]}$	0.0

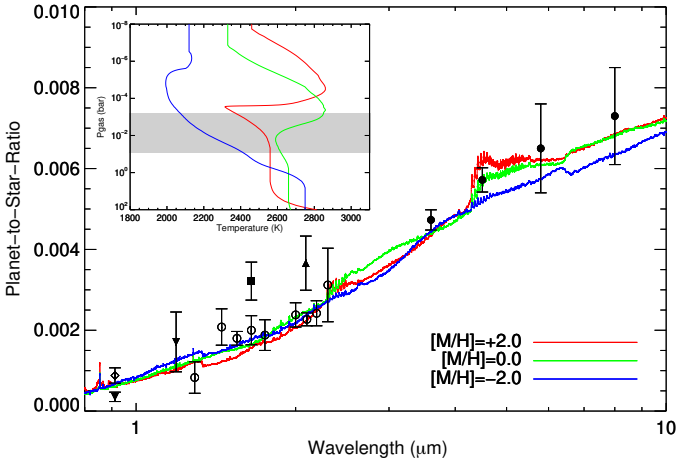

Fig. 1. Comparison of observed thermal spectra of WASP-19b with the modelled spectra calculated using PHOENIX (solid line) at different metallicities with an average dayside heat redistribution ($f = 0.5$). The corresponding temperature-pressure profile is shown in the inset image (the grey shaded region corresponds to the structure inversion). The observed thermal spectrum of WASP-19b presented in this paper is adopted from Anderson et al. (2010, 2013) (filled square and filled circles), Gibson et al. (2010) (filled upward triangle), Bean et al. (2013) (open circles), Burton et al. (2012) (open diamond), and Lendl et al. (2013) (filled downward triangles). The emission features at 4.5 μm are due to CO in the presence of thermal inversion.

namely at 5.8 and 8.0 μm, the planet-to-star flux ratio is even higher than 4.5 μm. This clearly indicates the presence of excess emission in some photometric bands over others.

The atmosphere of WASP-19b has been modelled with the parameters given in Table 1 using PHOENIX. It shows the presence of thermal inversion (see inset diagram, Fig. 1) and the equilibrium temperature is found to be ~2700 K. The comparison between observational data and our theoretical modelling (see Fig. 1) indicates that the excess planet-to-star flux ratio at 4.5 μm is due to the presence of CO, which in turn is caused by thermal inversion that exists in the atmosphere. The corresponding pressure range, as probed by the secondary eclipse, is 10^{-2} to 10^{-3} bar. Previous studies of WASP-19b did not show any evidence of thermal inversion in its atmosphere (Anderson et al. 2013; Bean et al. 2013). However, these studies were mainly based on retrieval techniques where abundances and thermal structure were fitted to the data.

We investigate the effect of metallicity on the atmosphere of WASP-19b by changing all the heavy-elemental abundances by a factor of two. As shown by the inset image of Fig. 1, the thermal inversion becomes stronger as the metallicity increases. This is mainly due to the temperature dependence of the thermal dissociation of various molecules, which changes the photospheric abundances ratio of TiO and H_2O at different metallicities (Parmentier et al. 2018). At higher metallicities, the increase in the abundances of various absorbers such as TiO warms the upper atmosphere. This causes the thermal inversion to be even stronger as compared to solar metallicity, which leads to strong emission features of CO and shallower features of H_2O in their thermal spectra. We find that models with sub-solar metallicities show the signature of very weak or no thermal inversion (see Fig. 1). This is a result of the decrease of TiO and VO abundances. In most of the hot Jupiters or massive planets, the metallicity is believed to approach the metallicity of the host star (Torres et al. 2012; Arcangeli et al. 2018). We also investigated this by comparing the observed thermal spectra of the dayside atmosphere of WASP-19b with the models at [M/H] = −2.0, 0.0 and +2.0. Our results show that thermal spectra of WASP-19b can be explained with a model at solar metallicity with thermal inversion, without invoking unusual abundances.

In the case of ultra-hot Jupiters, the molecular species required to explain the featureless observations are physically plausible. At extremely high temperature, the various molecules responsible for the radiative cooling in their atmosphere do not exist. In Fig. 2, we show the mixing ratio of the most important atomic and molecular species in the atmosphere of WASP-19b at different metallicities as a function of optical depth and temperature. We see that H_2 dissociates in the upper atmosphere due to impinging radiation from about $\tau = 10^{-2}$, but not enough to prevent the molecular hydrogen atmosphere. Due to the impinging radiation, free electrons are available and constant over most of the upper photosphere. Neutral atomic oxygen is fully locked to the very stable CO molecule in the deep atmosphere ($P > 10^{-2}$ bar), but becomes as abundant as CO in the upper atmosphere. This is the result of partial dissociation of CO, and other oxygen–bearing molecules. While CO is quasi-constant throughout the atmosphere. We find that H_2 and CO are the most abundant molecules, while CO, TiO, and VO are the most important molecular opacity sources in the atmosphere of WASP-19b.

As shown in Fig. 2 (left panels), we find that the variation of atomic and molecular abundances, together with the strong impinging radiation, contribute to the thermal inversion in the atmosphere of WASP-19b. At 0.0163 AU, the thermal structure of WASP-19b is too hot for the formation of BT-Settl clouds, whereas the presence of CO/CO_2 reveals the disequilibrium chemistry. We find the formation of a limited amount of CO_2 in disequilibrium chemistry, but it is not abundant enough to participate significantly in the CO and H_2O balance. We also show that TiO and alkali doublets, seen in early to mid-type brown dwarfs, are the main opacities in the optical to NIR spectrum of WASP-19b. It is evident from Fig. 2 (right panels) that the temperature inversion causes the wiggles in the concentrations along the structure, causing CO bands to appear in emission.

Figure 3 shows the synthetic spectra of WASP-19b in the optical at different metallicities. We see that despite extremely low abundances, similar to brown dwarfs and irradiated hot-Jupiter atmospheres (Allard et al. 2001; Barman et al. 2001, 2002), the TiO cross sections are strong enough to preserve TiO as the main optical to NIR opacity, along with alkali atomic fundamental transitions. These are the most important opacity sources, together with CO in the infrared, that survive the immense heat impinging on the planet's atmosphere the planet atmosphere. The thermal inversion potentially hides

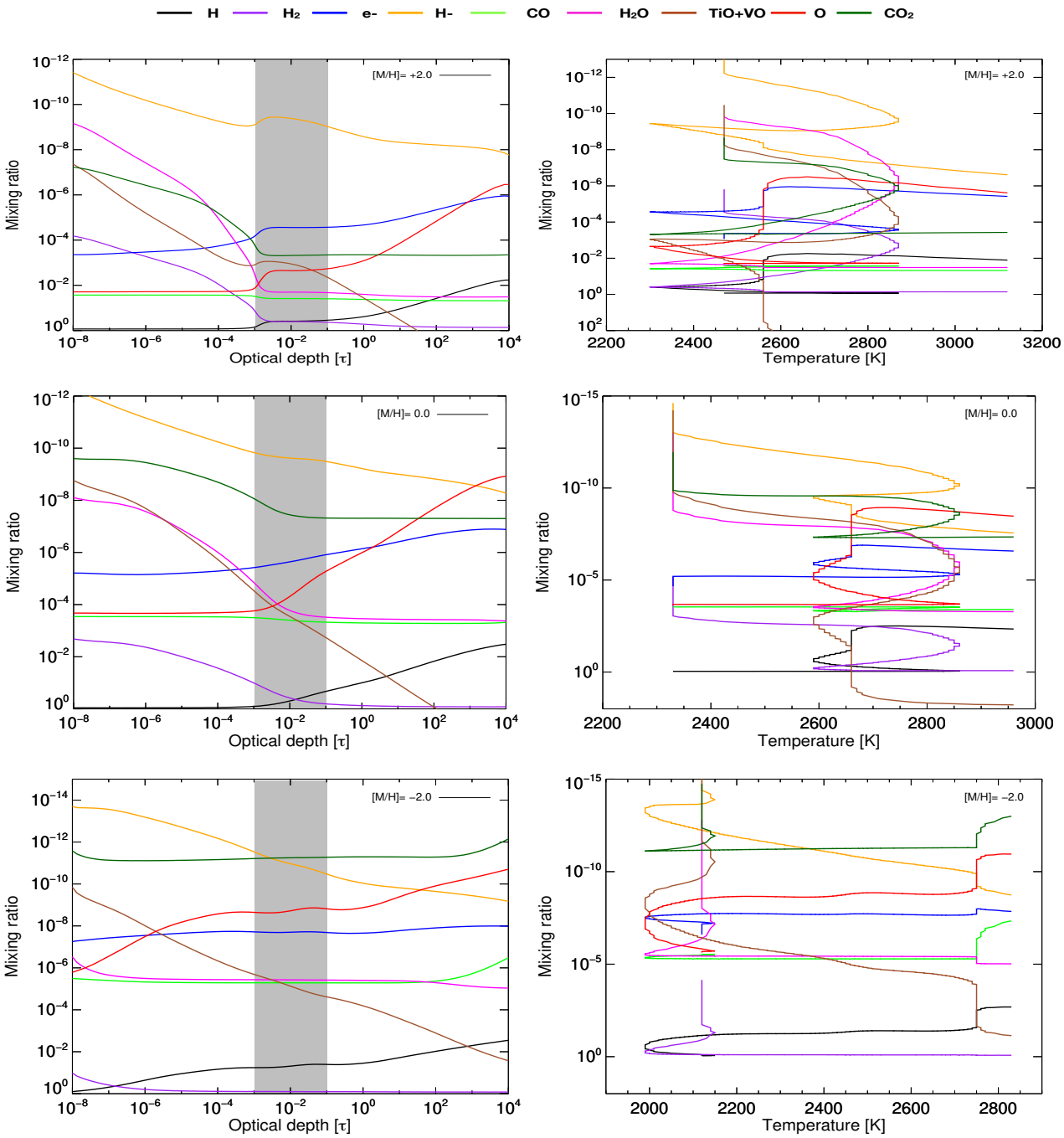

Fig. 2. Concentration of important absorbing molecules and neutral atoms as a function of optical depth and temperature at [M/H] = +2.0 (*top*), [M/H] = 0.0 (*middle*), and [M/H] = −2.0 (*bottom*). These species deplete at the given pressure range for the irradiated hot Jupiter WASP-19b (see main text). The grey shaded region (*left panels*) corresponds to the structure inversion and shows the window of the observable atmosphere from which most of the spectrum emerges (in the CO, H_2O, and TiO molecular bands pseudo-continuum). We notice that in the upper atmosphere ($\tau < 10^{-2}$), H_2O, TiO, and VO dissociate whereas neutral atomic oxygen remains constant. We find that CO remains constant throughout the atmosphere of WASP-19b. The temperature inversion (*right panels*) causes the wiggles along the structure, causing CO bands to emerge in emission.

pseudo-continuum opacities such as H_2O, and the high temperatures do not allow triatomic molecule to remain stable. Also at the given resolution and at such high temperature conditions, H_2O has a much flatter opacity profile making it more difficult to recognise, especially at those spectral resolutions.

4. Conclusions

We have used the state-of-the-art 1D NLTE opacity sampling model atmosphere code PHOENIX to study the atmosphere of WASP-19b. This model has been successfully used to study the atmosphere of cool stars, brown dwarfs, and extrasolar planets. The temperature-pressure profile of WASP-19b computed using PHOENIX shows the presence of thermal inversion. Our model computed at solar metallicity successfully reproduces the observed photometry of WASP-19b without the need for non-solar composition. The secondary eclipse of WASP-19b shows evidence for CO emission features at 4.5 μm, but no sign of H_2O. We find that these features are the result of thermal dissociation and thermal inversion due to the strong impinging

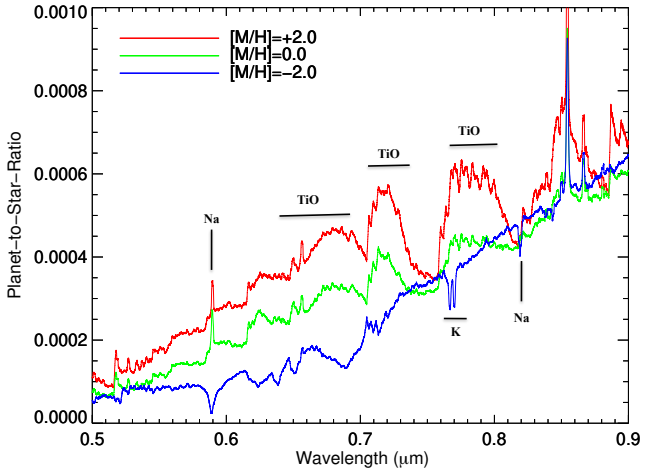

Fig. 3. Synthetic spectra of WASP-19b in the optical range calculated using PHOENIX at different metallicities with an average dayside heat redistribution ($f = 0.5$). Labels of the most prominent atomic and molecular features that remain important opacity sources, even at low concentrations, are indicated.

radiation. Also, the H_2O pseudo-continuum is much smoother at the concerned temperatures and densities, making it more difficult to identify at those extremely coarse spectral resolutions. Our results further strengthen the fact that the family of ultra-hot Jupiters commonly exhibit thermal inversions.

At longer wavelengths (above 1.4 μm) and at extremely hot temperatures (2200–2800 K), a significant amount of H_2O gets thermally dissociated at a pressure below 10^{-2} bar. At a temperature above 2200 K, TiO and VO do remain important opacity sources, even at low concentrations. At longer wavelengths, CO is the only molecule, with its strong triple bond, to be abundant below 10^{-2} bar. This molecule does not dissociate and its emission features appear at 4.5 μm. We suggest that the actual reason for the drop in H_2O in ultra-hot Jupiters is the partial thermal dissociation of this molecule and the resulting thermal inversion, which shapes the thermal spectra of ultra-hot Jupiters. This makes H_2O a poor diagnostic of the C/O ratio. Also at such high dayside temperatures (>2200 K), and at that resolution, the opacity profile of H_2O is spectrally much flatter and difficult to recognise.

Acknowledgements. We thank the anonymous referee for providing comments and suggestions which helped improve the clarity and conciseness of the paper. A.S.R. is grateful to Mudit Kumar Srivastava from Physical Research Laboratory (PRL) for providing feedback on the manuscript. The computations were performed on the HPC resources at the Physical Research Laboratory (PRL). The research leading to these results has received funding from the French "Programme National de Physique Stellaire" and the Programme National de Planetologie of CNRS (INSU). The computations were performed at the Pôle Scientifique de Modélisation Numérique (PSMN) at the École Normale Supérieure (ENS) in Lyon, and at the Gesellschaft für Wissenschaftliche Datenverarbeitung Göttingen in collaboration with the Institut für Astrophysik Göttingen. O.M. acknowledges support from CNES.

References

Allard, F., Hauschildt, P. H., Alexander, D. R., Tamanai, A., & Schweitzer, A. 2001, ApJ, 556, 357
Allard, F., Allard, N. F., Homeier, D., et al. 2007, A&A, 474, L21
Allard, F., Homeier, D., Freytag, B., & Sharp, C. M. 2012, EAS Pub. Ser., 57, 3
Allard, F., Homeier, D., Freytag, B., et al. 2013, Mem. Soc. Astron. It. Suppl., 24, 128
Anderson, D. R., Gillon, M., Maxted, P. F. L., et al. 2010, A&A, 513, L3
Anderson, D. R., Smith, A. M. S., Madhusudhan, N., et al. 2013, MNRAS, 430, 3422
Arcangeli, J., Désert, J.-M., Line, M. R., et al. 2018, ApJ, 855, L30
Barklem, P. S., Piskunov, N., & O'Mara, B. J. 2000, A&A, 363, 1091
Barman, T. 2007, ApJ, 661, L191
Barman, T. S., Hauschildt, P. H., & Allard, F. 2001, ApJ, 556, 885
Barman, T. S., Hauschildt, P. H., Schweitzer, A., et al. 2002, ApJ, 569, L51
Bean, J. L., Désert, J.-M., Seifahrt, A., et al. 2013, ApJ, 771, 108
Beatty, T. G., Madhusudhan, N., Pogge, R., et al. 2017a, AJ, 154, 242
Beatty, T. G., Madhusudhan, N., Tsiaras, A., et al. 2017b, AJ, 154, 158
Burrows, A., Sudarsky, D., & Hubeny, I. 2004, ApJ, 609, 407
Burrows, A., Budaj, J., & Hubeny, I. 2008, ApJ, 678, 1436
Burton, J. R., Watson, C. A., Littlefair, S. P., et al. 2012, ApJS, 201, 36
Butler, R. P., Wright, J. T., Marcy, G. W., et al. 2006, ApJ, 646, 505
Caffau, E., Ludwig, H.-G., Steffen, M., Freytag, B., & Bonifacio, P. 2011, Sol. Phys., 268, 255
Charbonneau, D., Brown, T. M., Noyes, R. W., & Gilliland, R. L. 2002, ApJ, 568, 377
Désert, J. M., Vidal-Madjar, A., Lecavelier Des Etangs, A., et al. 2008, A&A, 492, 585
Diamond-Lowe, H., Stevenson, K. B., Bean, J. L., Line, M. R., & Fortney, J. J. 2014, ApJ, 796, 66
Evans, T. M., Sing, D. K., Kataria, T., et al. 2017, Nature, 548, 58
Fortney, J. J., Sudarsky, D., Hubeny, I., et al. 2003, ApJ, 589, 615
Fortney, J. J., Lodders, K., Marley, M. S., & Freedman, R. S. 2008, ApJ, 678, 1419
Gibson, N. P., Aigrain, S., Pollacco, D. L., et al. 2010, MNRAS, 404, L114
Graven, W. M., & Long, F. J. 1954, J. Am. Chem. Soc., 76, 2602
Haynes, K., Mandell, A. M., Madhusudhan, N., Deming, D., & Knutson, H. 2015, ApJ, 806, 146
Hebb, L., Collier-Cameron, A., Triaud, A. H. M. J., et al. 2010, ApJ, 708, 224
Hellier, C., Anderson, D. R., Collier-Cameron, A., et al. 2011, ApJ, 730, L31
Kitzmann, D., Heng, K., Rimmer, P. B., et al. 2018, ApJ, 863, 183
Knutson, H. A., Howard, A. W., & Isaacson, H. 2010, ApJ, 720, 1569
Kreidberg, L., Line, M. R., Parmentier, V., et al. 2018, AJ, 156, 17
Lendl, M., Gillon, M., Queloz, D., et al. 2013, A&A, 552, A2
Line, M. R., & Parmentier, V. 2016, ApJ, 820, 78
Line, M. R., Wolf, A. S., Zhang, X., et al. 2013, ApJ, 775, 137
Lothringer, J. D., Barman, T., & Koskinen, T. 2018, ApJ, 866, 27
Madhusudhan, N. 2012, ApJ, 758, 36
Madhusudhan, N., & Seager, S. 2009, ApJ, 707, 24
Madhusudhan, N., Knutson, H., Fortney, J. J., & Barman, T. 2014, in Protostars and Planets VI, eds. H. Beuther, R. S. Klessen, C. P. Dullemond, & T. Henning (Tucson, AZ; University of Arizona Press), 739
Mansfield, M., Bean, J. L., Line, M. R., et al. 2018, AJ, 156, 10
Nugroho, S. K., Kawahara, H., Masuda, K., et al. 2017, AJ, 154, 221
Parmentier, V., Showman, A. P., & Lian, Y. 2013, A&A, 558, A91
Parmentier, V., Fortney, J. J., Showman, A. P., Morley, C., & Marley, M. S. 2016, ApJ, 828, 22
Parmentier, V., Line, M. R., Bean, J. L., et al. 2018, A&A, 617, A110
Rajpurohit, A. S., Reylé, C., Schultheis, M., et al. 2012, A&A, 545, A85
Sedaghati, E., Boffin, H. M. J., MacDonald, R. J., et al. 2017, Nature, 549, 238
Sheppard, K. B., Mandell, A. M., Tamburo, P., et al. 2017, ApJ, 850, L32
Southworth, J., Wheatley, P. J., & Sams, G. 2007, MNRAS, 379, L11
Spiegel, D. S., Silverio, K., & Burrows, A. 2009, ApJ, 699, 1487
Stevenson, K. B., Bean, J. L., Madhusudhan, N., & Harrington, J. 2014, ApJ, 791, 36
Swain, M., Deroo, P., Tinetti, G., et al. 2013, Icarus, 225, 432
Tinetti, G., Vidal-Madjar, A., Liang, M.-C., et al. 2007, Nature, 448, 169
Torres, G., Fischer, D. A., Sozzetti, A., et al. 2012, ApJ, 757, 161
Unsold, A. 1968, Physik der Sternatmospharen, MIT besonder Berucksichtigung der Sonne
Valenti, J. A., & Piskunov, N. 1996, A&AS, 118, 595
Visscher, C., Moses, J. I., & Saslow, S. A. 2010, Icarus, 209, 602
Zellem, R. T., Swain, M. R., Roudier, G., et al. 2017, ApJ, 844, 27